THE DISCOVERY OF A RADIO HALO IN PLCK G147.3–16.6 AT $Z = 0.65$

R. J. van Weeren[1,*], H. T. Intema[2], D. V. Lal[3], A. Bonafede[4], C. Jones[1], W. R. Forman[1], H. J. A. Röttgering[5], M. Brüggen[4], A. Stroe[5], M. Hoeft[6], S. E. Nuza[7], and F. de Gasperin[4]

[1]Harvard-Smithsonian Center for Astrophysics, 60 Garden Street, Cambridge, MA 02138, USA
[2]National Radio Astronomy Observatory, 1003 Lopezville Road, Socorro, NM 87801-0387, USA
[3]National Centre for Radio Astrophysics, TIFR, Pune University Campus, Post Bag 3, Pune 411 007, India
[4]Hamburger Sternwarte, Gojenbergsweg 112, 21029 Hamburg, Germany
[5]Leiden Observatory, Leiden University, P.O. Box 9513, NL-2300 RA Leiden, The Netherlands
[6]Thüringer Landessternwarte Tautenburg, Sternwarte 5, 07778, Tautenburg, Germany and
[7] Leibniz-Institut für Astrophysik Potsdam (AIP), An der Sternwarte 16, 14482 Potsdam, Germany
Draft version October 13, 2018

ABSTRACT

Recent X-ray and Sunyaev-Zel'dovich (SZ) observations have dramatically increased the number of known distant galaxy clusters. In some merging, low-redshift ($z < 0.4$) clusters, centrally-located, diffuse, extended radio emission (called radio halos) has been found. Using the Giant Metrewave Radio Telescope (GMRT), we report the detection of diffuse radio emission in the binary-merging cluster PLCK G147.3–16.6 located at $z = 0.65$. We classify the emission as a giant radio halo due to the large physical extent of about 0.9 Mpc and low-surface brightness. We measure an integrated flux density of 7.3 ± 1.1 mJy at 610 MHz for the radio halo, resulting in a 1.4 GHz radio power of 5.1×10^{24} W Hz^{-1}. The radio halo power is consistent with that expected from the known correlation between X-ray luminosity or the cluster integrated SZ signal and radio power. Our observations also suggest that more of these distant radio halos could be discovered with the GMRT.

Subject headings: Galaxies: clusters: individual (PLCK G147.3–16.6) — Galaxies: clusters: intracluster medium — large-scale structure of universe — Radiation mechanisms: non-thermal — X-rays: galaxies: clusters

1. INTRODUCTION

In some merging galaxy clusters, Mpc-scale diffuse radio synchrotron emission is found, which indicates the presence of relativistic particles and magnetic fields in the intracluster medium (ICM). The diffuse emission is classified depending on the location, morphology, and polarization properties (see Feretti et al. 2012, for a recent review).

Radio halos have sizes of about a Mpc and are centrally located in clusters (e.g. Brown & Rudnick 2011). It has been proposed that radio halos trace particles re-accelerated by turbulence generated during a cluster merger event (Brunetti et al. 2001; Petrosian 2001). In an alternative model, radio halos are produced by secondary electrons injected during proton-proton collisions in the ICM (e.g., Dennison 1980; Blasi & Colafrancesco 1999; Dolag & Enßlin 2000; Miniati et al. 2001; Keshet & Loeb 2010). Secondary models are challenged by the large energy content of cosmic ray protons needed to explain radio halos with very steep spectra (e.g., Brunetti et al. 2008) and by the non-detection of γ-rays from radio halos (e.g., Jeltema & Profumo 2011; Brunetti et al. 2012).

For radio halos there is a correlation between X-ray luminosity and radio power/luminosity (the $L_{\rm X} - P$ correlation), with the most luminous clusters hosting the most powerful radio halos (e.g., Liang et al. 2000; Enßlin & Röttgering 2002; Cassano et al. 2006). There

E-mail: rvanweeren@cfa.harvard.edu
* Einstein Fellow

is also a strong bimodality observed in the $L_{\rm X} - P$ plane. Merging clusters that host radio halos follow the $L_{\rm X} - P$ scaling relation, while for other relaxed clusters the upper limits on the radio power are well below the correlation (Brunetti et al. 2007). The radio halo power also correlates with the integrated Sunyaev-Zel'dovich (SZ) effect signal (Basu 2012, 2013; Cassano et al. 2013) given by the Compton $Y_{\rm SZ}$ parameter, which traces the integrated pressure along the line of sight. The SZ signal is expected to be a better indicator of cluster mass than the X-ray luminosity and should be less affected by the cluster dynamical state. In addition, there are indications that the fraction of clusters with diffuse radio emission is larger for SZ selected samples (Sommer & Basu 2013), which suggests that X-rays and SZ statistics provide complementary information on the radio-merger connection.

The majority of the presently known halos and relics are located at low and moderate redshifts ($z \lesssim 0.4$). Not much is known about the radio relic and halo population beyond $z \gtrsim 0.6$, with only a one cluster known that hosts diffuse radio emission at $z = 0.87$ (Menanteau et al. 2012; Lindner et al. 2013) and two around a redshift of 0.55 (Edge et al. 2003; van Weeren et al. 2009; Bonafede et al. 2009, 2012). Radio halos and relics are in general difficult to study owing to their low surface brightness and steep radio spectrum, making them faint at high frequencies. Since they are already difficult to detect in nearby clusters, only the most luminous ones can be detected beyond $z \gtrsim 0.6$. According to the $L_{\rm X}-P$ correlation the most luminous halos are located in the most massive (i.e., X-ray luminous) clusters. We have there-

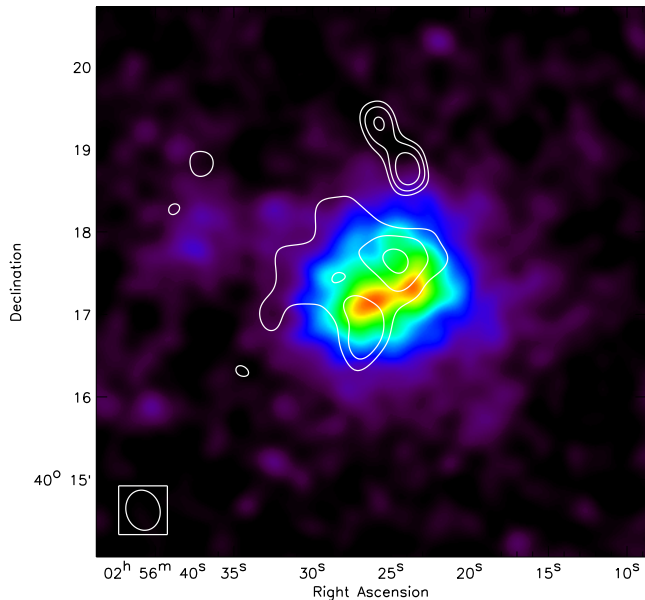FIG. 1.— XMM-Newton 0.5–3.0 keV X-ray image of PLCK G147.3–16.6 convolved with a 16″ FWHM Gaussian. Radio contours from the low-resolution GMRT 610 MHz image (Fig. 2; right panel) are overlaid in white. Contour levels are drawn at $\sqrt{[1, 2, 4, 8, \ldots]} \times 3\sigma_{\rm rms}$, with $\sigma_{\rm rms} = 0.175$ mJy beam^{-1}.

fore started to observe a sample of massive $z \gtrsim 0.6$ clusters with the Giant Metrewave Radio Telescope (GMRT) to carry out a first systematic characterization of the distant halo (and relic) population. In this letter we report the discovery of diffuse emission in the merging cluster PLCK G147.3–16.6 at $z = 0.65$.

Throughout this letter we assume a ΛCDM cosmology with $H_0 = 71$ km s^{-1} Mpc^{-1}, $\Omega_m = 0.27$, and $\Omega_\Lambda = 0.73$. With the adopted cosmology, $1''$ corresponds to a physical scale of 6.9 kpc at $z = 0.65$ (Wright 2006). All images are in the J2000 coordinate system.

2. OBSERVATIONS & DATA REDUCTION

PLCK G147.3–16.6 was observed for 8 hrs with the GMRT on Jan. 18, 2013 at 610 MHz. Both the RR and LL correlations were recorded. We used an integration time of 8 s and, after splitting of noisy edge channels, obtained 29 MHz of usable bandwidth. The data were reduced using a semi-automatic pipeline employing the Astronomical Image Processing System[2] (AIPS), ParselTongue and Obit (Cotton 2008). The reduction consisted of automatic RFI removal and subtraction (Athreya 2009), bandpass and gain calibration, and subsequent cycles of self-calibration. In addition, direction dependent phase solutions were obtained to employ the Source Peeling and Atmospheric Modeling ionospheric calibration scheme (Intema et al. 2009). Sources with a signal to noise ratio > 1000 had their own individual direction dependent gain solutions applied. The flux-scale for the primary calibrator 3C147 was set according to the Scaife & Heald (2012) flux scale. For the imaging, facets were used to correct for the non-coplanar nature of the array and to apply the direction dependent calibration solutions.

We used archival i-band images taken with the DO-LORES (Device Optimized for the LOw RESolution)

instrument on the Telescopio Nazionale Galileo (TNG) telescope at La Palma. The 2048×2048 pixel images have a scale of $0.252''$ per pixel. We combined 10 images with a total exposure time of 3000 s using IRAF. We used a 100 pixel medium filter to self-flatten the images as no i-band flat field images were found for the night of the observing run. XMM-Newton archival observations (ObsID: 0679181301) of the cluster were reduced with the Science Analysis Software[3] (SAS, v13.0), resulting in a net clean exposure time of about 10.2 ks. Periods with high background counts were filtered using the tasks pn-$filter$ and mos-$filter$. We made an exposure-corrected MOS+pn image in the 0.5–3.0 keV band, see Fig. 1.

3. PLCK G147.3–16.6

PLCK G147.3–16.6 was confirmed to be a cluster by the Planck Collaboration et al. (2013). Based on XMM-Newton spectra, a redshift of 0.62 was found using the Fe K line. The cluster has an X-ray luminosity of $7.15 \pm 0.66 \times 10^{44}$ erg $^{-1}$ within R_{500} in the 0.1–2.4 keV band. Spectroscopic observations obtained with Gemini North GMOS-N of about a dozen candidate cluster members resulted in a redshift of 0.66 ± 0.05 for the cluster. Excluding two galaxies at $z = 0.68$, the Planck Collaboration et al. (2013) give a redshift of 0.645 ± 0.005. Their optical imaging shows a complex galaxy distribution, without a single dominant cD galaxy. The XMM observations reveal two peaks/substructures in the X-ray surface brightness separated by ~ 250 kpc (see Fig. 1), which roughly coincide with the observed galaxy distribution. There are hints that the X-ray surface brightness distribution is more complex as the eastern substructure is more elongated than the western one. The Planck Collaboration et al. (2013) reported a global temperature (T_{500}) of 8.8 ± 0.8 keV using the XMM data. Both the optical and X-ray data indicate that PLCK G147.3–16.6 is undergoing a merger event. A summary of the cluster's properties is given in Table 1.

4. RESULTS

TABLE 1
CLUSTER AND RADIO HALO PROPERTIES

z	0.645 ± 0.005^a
R_{500} (kpc)	1042
$L_{\rm X,500}$ (10^{44} erg s^{-1}, 0.1–2.4 keV)	7.15 ± 0.66
Y_{500} (10^{-4} arcmin^2)	5.2 ± 1.7^b
T_{500} (keV)	8.8 ± 0.8
M_{500} (10^{14} M$_\odot$)	6.3 ± 0.4
$S_{\rm halo,610MHz}$ (mJy)	7.3 ± 1.1
$P_{\rm halo,1.4GHz}$ (10^{24} W Hz^{-1})	5.1 ± 0.8^c
$R_{\rm halo}$ (Mpc)	0.9
Compact source fluxes (mJy)	2.42 ± 0.25 (A)
	1.63 ± 0.18 (B)
	0.88 ± 0.29 (C)
	0.38 ± 0.09 (D)
	0.31 ± 0.08 (E)
	0.19 ± 0.07 (F)

^{a} see the Planck Collaboration et al. (2013) for a discussion on the redshift
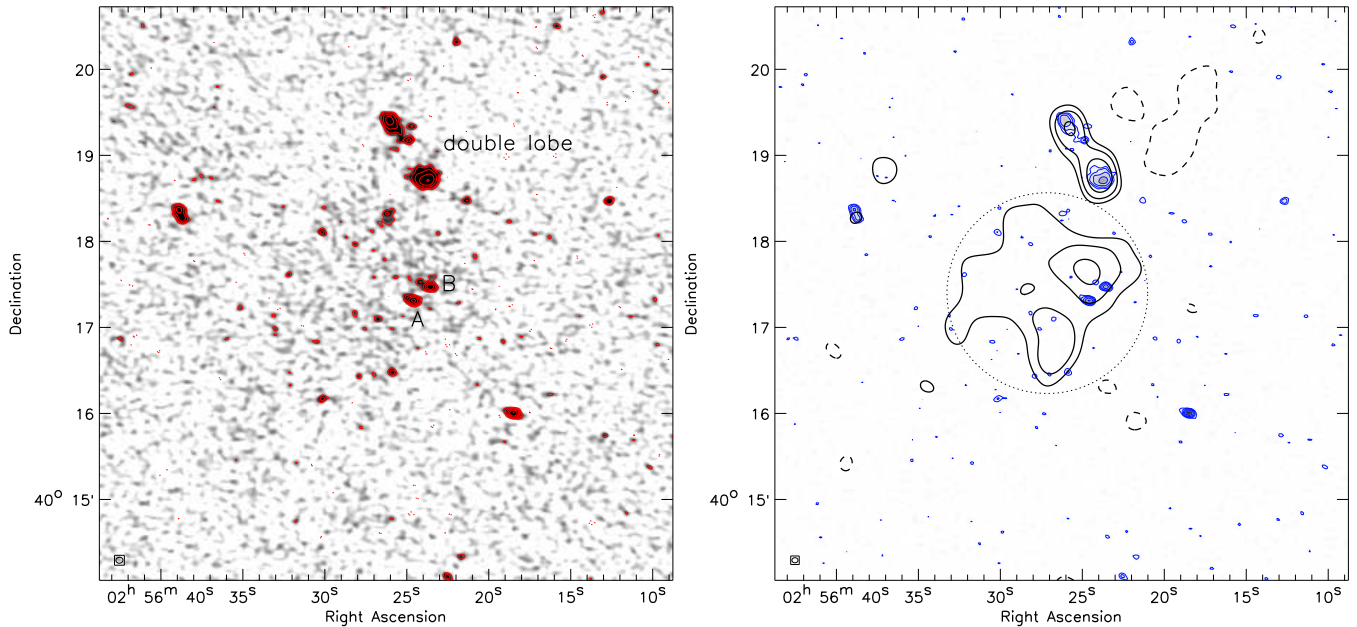^{b} $0.89 \pm 0.29 \times 10^{-4}$ Mpc^2

FIG. 2.— Left: GMRT 610 MHz image (using all data). Contour levels are drawn at $[-1, 1, 2, 4, 8, \ldots] \times 3\sigma_{\rm rms}$, with $\sigma_{\rm rms} = 38\ \mu$Jy beam^{-1}. Negative contours are shown by the dotted lines. Source A and B, both cluster members, are indicated. Right: A low-resolution $30'' \times 25''$ image of the cluster with the emission from compact sources subtracted. Contours are drawn at $\sqrt{[1, 2, 4, 8, \ldots]} \times 3\sigma_{\rm rms}$, with the 2.5σ negative contours show by the dashed lines and $\sigma_{\rm rms} = 0.175$ mJy beam^{-1}. The high-resolution image ($4.3'' \times 3.6''$, indicated in the bottom left corner), made by excluding data below 2 kλ, is shown with blue contours. Contours levels are drawn at $[1, 2, 4, 8, \ldots] \times 3\sigma_{\rm rms}$ ($\sigma_{\rm rms} = 43\ \mu$Jy beam^{-1}), this emission was subtracted before making the low-resolution image. The dotted circle indicates the area for which we performed the integrated flux measurement.

^{c} assuming a spectral index of $\alpha = -1.3$ for the radio halo, with $F_\nu \propto \nu^\alpha$

Our GMRT 610 MHz image of the cluster is shown in Fig. 2 (left panel). This image was made with Briggs weighting (Briggs 1995) using a robust value of -1, giving a resolution of $4.9'' \times 4.2''$. Several compact radio sources are visible as well as a double lobe source just to the north of the cluster, with the two lobes separated by about $1'$. Two relatively bright compact sources are located in the central region of the cluster. We identify optical counterpart for these sources in the TNG i-band image, see Fig. 3. Source A is a spectroscopically confirmed cluster member. Source B is associated with the cD galaxy of the western subcluster. This galaxy is a cluster member given the very similar color to the other clusters members in fig. 3 from the Planck Collaboration et al. (2013). Besides A and B, a few other fainter sources are present (see Fig. 3). The flux densities of these sources are reported in Table 1.

A careful visual inspection of the image reveals an increase in the "noise" at the cluster position, hinting at a large extended low-surface brightness component. To make this emission more visible, we subtracted the emission from compact radio sources from the uv-data. For this, we first made a high-resolution image by excluding data below 2 kλ (corresponding to a angular scale of about $2'$). This image is shown in Fig. 2 (right panel). We subtracted the clean components obtained from this image from the uv-data. We then re-imaged the data, excluding data above 8 kλ and using a taper of 5 kλ (units are the distance to the 30% percent point of the Gaussian in kλ) to enhance diffuse emission. This resulted in an image with a resolution of $30'' \times 25''$. We verified that
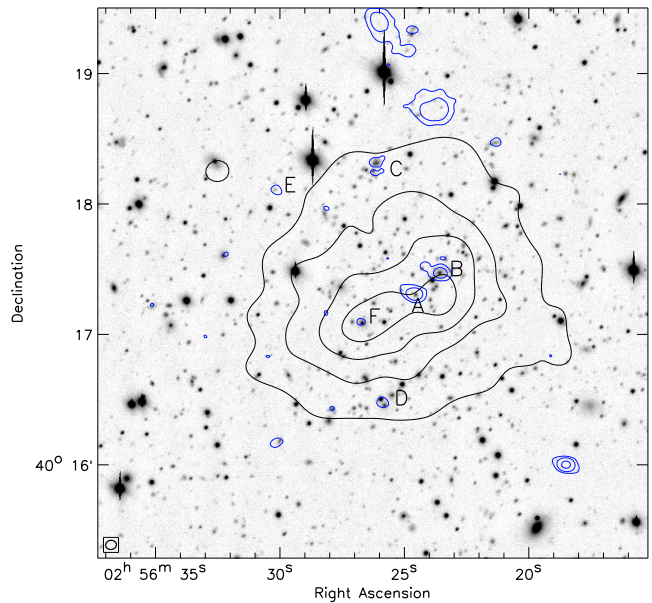

FIG. 3.— TNG/DOLORES i-band image of PLCK G147.3–16.6. XMM-Newton X-ray contours from Fig. 1 are overlaid in black. Radio contours from the high-resolution GMRT 610 MHz image (Fig. 2; left panel) are overlaid in blue. Compact sources are labelled. Contour levels are drawn at $[1, 4, 16, 64, \ldots] \times 4\sigma_{\rm rms}$. The beam size is $4.9'' \times 4.2''$ and indicated in the bottom left corner.

the source subtraction procedure did not leave any positive residuals, by visually inspecting the low-resolution image at the locations of several dozen compact sources that are located throughout the primary beam. We clearly detect diffuse emission at the cluster position with a total extent of about $2.2'$, corresponding to a physical extent ($R_{\rm halo}$) of 0.9 Mpc at the distance of the cluster.
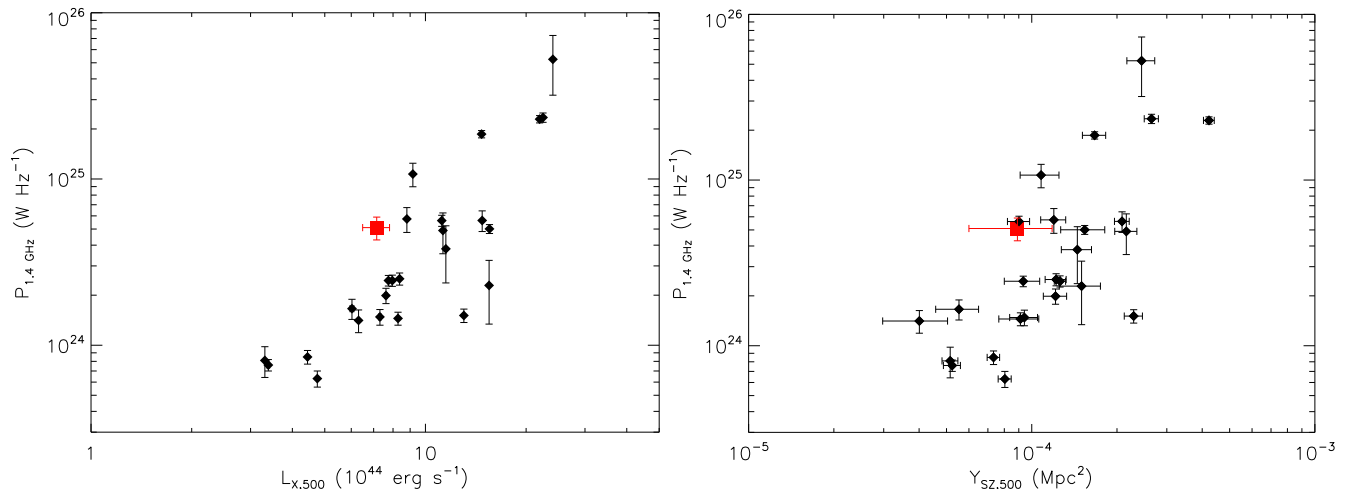
FIG. 4.— Left: Distribution of clusters in the $L_{\mathrm{X},500} - P_{1.4\ \mathrm{GHz}}$ plane. The data were taken from the list compiled by Cassano et al. (2013) and are plotted with black diamonds. The datapoint for PLCK G147.3–16.6 is indicated by a red square. Right: Distribution of clusters in the $Y_{\mathrm{SZ},500} - P_{1.4\ \mathrm{GHz}}$ plane. Labeling is the same as in the left panel. We conclude that the PLCK G147.3–16.6 radio halo power is what is expected from known $L_{\mathrm{X},500} - P_{1.4\ \mathrm{GHz}}$ and $Y_{\mathrm{SZ},500} - P_{1.4\ \mathrm{GHz}}$ correlations.

Some emission from the double lobe source to the north remains visible because of the extended nature of this source. Source C and F were not cleaned in the data with the short uv-spacings removed (Fig. 2; right panel), as their peak fluxes fall below the clean box threshold. After subtracting their contribution, we measure an integrated flux ($S_{610\mathrm{MHz}}$) of 7.3 ± 1.1 mJy for the diffuse emission, summing the emission in the circular region indicated in Fig. 2. The quoted uncertainty is based on a 10% absolute flux calibration uncertainty and the statistical uncertainty due to map noise, i.e., $(\sigma_{S_{610\mathrm{MHz}}})^2 = (0.1 S_{610\mathrm{MHz}})^2 + (\sigma_{\mathrm{rms}}\sqrt{\#\mathrm{beams\ in\ halo\ area}})^2$. We note that the actual uncertainty could be somewhat larger, as it is not fully clear what the area is over which we should integrate the halo flux.

In Fig. 1 we overlay the radio emission on an XMM MOS+pn 0.5–3.0 keV X-ray image. The radio emission roughly follows the X-ray emission, although the radio emission seems to be somewhat more extended in the northeast direction. It should be noted however that the radio emission has a very low surface brightness and therefore not too many conclusions should be drawn based on the brightness distribution. We classify the source as a radio halo, since the emission coincides with most of the X-ray emission from the ICM. In addition, the very low surface brightness is typical for a radio halo. The fact that the cluster is undergoing a merger, based on the optical and X-ray data, provides further support for this interpretation.

If we assume a spectral index of -1.3 for the radio halo (e.g., Feretti et al. 2012), we obtain a 1.4 GHz k-corrected radio power of $P_{1.4\ \mathrm{GHz}} = 5.1 \times 10^{24}$ W Hz^{-1}. It is thought that distant radio halos have on average steeper spectral indices than their low-z counterparts (e.g., Cassano et al. 2010). If we assume a spectral index of -1.8 this would result in a (k-corrected) radio power of 4.3×10^{24} W Hz^{-1}. This difference in the radio power between $\alpha = -1.3$ and -1.8 is thus about the same as the uncertainty introduced by the flux mea-

surement error. The position of PLCK G147.3–16.6 in the $L_{X,500} - P_{1.4\ \mathrm{GHz}}$ and $Y_{SZ,500} - P_{1.4\ \mathrm{GHz}}$ diagrams is shown in Fig. 4. Based on the $L_X - P_{1.4\ \mathrm{GHz}}$ correlation we would expect a power of about 2.3×10^{24} W Hz^{-1}, using the *BCES Bisector (RH only)* fit from Cassano et al. (2013, table 3). Given the intrinsic scatter in the correlation, measurement uncertainties and unknown spectral index, the observed radio power of PLCK G147.3–16.6 is consistent with being on the $L_X - P_{1.4\ \mathrm{GHz}}$ correlation. Based on the $Y_{SZ,500} - P_{1.4\ \mathrm{GHz}}$ *BCES Bisector (RH only)* fit from Cassano et al. (2013), we expect a radio power of 2.4×10^{24} W Hz^{-1}, almost the same as the prediction from the $L_X - P_{1.4\ \mathrm{GHz}}$ relation. Therefore, we conclude that the measured radio power is in agreement with that expected from the $L_X - P_{1.4\ \mathrm{GHz}}$ and $Y_{SZ} - P_{1.4\ \mathrm{GHz}}$ correlations.

5. CONCLUSIONS

We have discovered diffuse radio emission in the cluster PLCK G147.3–16.6 with the GMRT at 610 MHz. We classify this diffuse emission as a 0.9 Mpc radio halo. For the radio halo we measure an integrated flux of 7.3 ± 1.1 mJy, resulting in a radio power of $P_{1.4\ \mathrm{GHz}} = 5.1 \times 10^{24}$ W Hz^{-1} at the redshift of 0.65. This value is in agreement with what is expected from the known correlations between X-ray luminosity and SZ signal and radio power.

The detection of radio halos beyond $z \gtrsim 0.6$ has generally been considered more difficult because of the strong increase of the inverse Compton (IC) losses with redshift, which decreases the radio halo power. In addition, distant halos are expected to have steeper spectral indices than their low-z counterparts (e.g., Cassano et al. 2010). This is caused by the increase of the IC losses with redshift, which limit the maximum energy of the accelerated electrons in these systems, and the assumption the radio halo spectra have convex shapes as stochastic particle acceleration by MHD turbulence is believed to be an inefficient process. The detection of a radio halo in PLCK G147.3–16.6 at $z = 0.65$ now opens up the

exciting opportunity to study a radio halo in a distant cluster in more detail. Deep follow-up studies with the Karl G. Jansky VLA and LOFAR will be pursued to determine the spectral index and polarization properties of the radio halo. Our observations also suggest that detection and initial studies of distant radio halos are within the capabilities of the GMRT and that we should expect additional detections from our larger sample.

REFERENCES

Athreya, R. 2009, ApJ, 696, 885

Basu, K. 2012, MNRAS, 421, L112

—. 2013, Astronomische Nachrichten, 334, 350

Blasi, P., & Colafrancesco, S. 1999, Astroparticle Physics, 12, 169

Bonafede, A., Feretti, L., Giovannini, G., et al. 2009, A&A, 503, 707

Bonafede, A., Brüggen, M., van Weeren, R., et al. 2012, MNRAS, 426, 40

Briggs, D. S. 1995, PhD thesis, New Mexico Institute of Mining Technology, Socorro, New Mexico, USA

Brown, S., & Rudnick, L. 2011, MNRAS, 412, 2

Brunetti, G., Giacintucci, S., Cassano, R., et al. 2008, Nature, 455, 944

Brunetti, G., Blasi, P., Reimer, O., et al. 2012, MNRAS, 426, 956

Brunetti, G., Setti, G., Feretti, L., & Giovannini, G. 2001, MNRAS, 320, 365

Brunetti, G., Venturi, T., Dallacasa, D., et al. 2007, ApJ, 670, L5

Cassano, R., Brunetti, G., Röttgering, H. J. A., & Brüggen, M. 2010, A&A, 509, A68+

Cassano, R., Brunetti, G., & Setti, G. 2006, MNRAS, 369, 1577

Cassano, R., Ettori, S., Brunetti, G., et al. 2013, ApJ, 777, 141

Cotton, W. D. 2008, PASP, 120, 439

Dennison, B. 1980, ApJ, 239, L93

Dolag, K., & Enßlin, T. A. 2000, A&A, 362, 151

Edge, A. C., Ebeling, H., Bremer, M., et al. 2003, MNRAS, 339, 913

Enßlin, T. A., & Röttgering, H. 2002, A&A, 396, 83

Feretti, L., Giovannini, G., Govoni, F., & Murgia, M. 2012, A&A Rev., 20, 54

Intema, H. T., van der Tol, S., Cotton, W. D., et al. 2009, A&A, 501, 1185

Jeltema, T. E. & Profumo, S. 2011, ApJ, 728, 53

Keshet, U., & Loeb, A. 2010, ApJ, 722, 737

Liang, H., Hunstead, R. W., Birkinshaw, M., & Andreani, P. 2000, ApJ, 544, 686

Lindner, R. R., Baker, A. J., Hughes, J. P., et al. 2013, ArXiv e-prints

Menanteau, F., Hughes, J. P., Sifón, C., et al. 2012, ApJ, 748, 7

Miniati, F., Jones, T. W., Kang, H., & Ryu, D. 2001, ApJ, 562, 233

Petrosian, V. 2001, ApJ, 557, 560

Planck Collaboration, Ade, P. A. R., Aghanim, N., et al. 2013, A&A, 550, A130

Scaife, A. M. M., & Heald, G. H. 2012, MNRAS, 423, L30

Sommer, M. W., & Basu, K. 2013, ArXiv e-prints

van Weeren, R. J., Röttgering, H. J. A., Brüggen, M., & Cohen, A. 2009, A&A, 505, 991

Wright, E. L. 2006, PASP, 118, 1711